ELSEVIER

Separation and Purification Technology 15 (1999) 41–58

Separation and Purification Technology

A study of the scale-up of reversed-phase liquid chromatography

T. Gu *, Y. Zheng [1]

Department of Chemical Engineering, Ohio University, Athens, OH 45701, USA

Received 21 May 1996; received in revised form 10 April 1998; accepted 8 May 1998

corrected

Abstract

A general rate model for liquid chromatography which considers nonlinear isotherms and various mass transfer effects, including axial dispersion, interfacial film mass transfer and intraparticle diffusion is applied to the modeling and scale-up of reversed-phase liquid chromatography. The model is solved with a FORTRAN program which is run on a personal computer. With a few simple experiments using a small analytical column, the binding characteristics and the porosity of the packing particles are determined. Mass transfer parameters are evaluated using existing correlations in the literature without any experimentation. Human growth hormone and a recombinant human growth hormone analog (hGHG120R) were used as protein samples in experiments. Gradient elution profiles of a preparative column are predicted without a posteriori data.

Keywords: Chromatography; Gradient; Model; Reversed phase; Scale-up

1. Introduction

Reversed-phase high-performance liquid chromatography (RP-HPLC) separates proteins based on the hydrophobic interaction between the protein molecules and the stationary phase. It is a very important analytical tool in modern biotechnology. It is also used at preparative- and large-scales for protein purification. In gradient elution, a modulator is used in the mobile phase to adjust the eluent strength. The most commonly used modulator in RP-HPLC is acetonitrile (ACN). In portein purification, gradient elution is used much more often than isocratic elution, since proteins have a wide range of retentivity [1]. In preparative- and large-scale operations, gradient elution can concentrate a dilute sample and achieve purification at the same time. An isocratic elution always dilutes a sample to a certain degree after a purification. The sample volume in isocratic elution is limited to a small fraction of the column bed volume, while in gradient elution, the sample volume can be many times that of the column bed volume. Thus, gradient elution is desired in the preparative- and large-scale purification of large samples.

Unlike analyticasl HPLC, which involves small and dilute samples separated on a highly efficient column, the column is often overloaded in terms of sample feed volume and/or concentration or both in preparative- and large-scale gradient elu-

* Corresponding author.

[1]Current address: R&D Department, U.S. Tobacco Manufacturing Company, 800 Harrison Street, Nashville, Tennessee 37203.

1383-5866/99/$ – see front matter
PII S1383-5866(99)00083-5

tion chromatography [2]. The column may not be a high-resolution column due to scale and cost considerations. Larger particle sizes may be used for column packing. In such cases, interference effects (binding competitions between different components), axial dispersion and mass transfer resistances such as interfacial film mass transfer and intraparticle diffusion may not be negligible.

The scale-up of protein purification using gradient elution was largely performed based on trial-and-error by experiments [3] with the help of some simple relationships which are no more than rules of thumb. The theoretical basis for gradient elution in nonlinear chromatography is quite complicated [4]. Because of the mathematical difficulties involved in the modeling of gradient elution, very few existing models consider interfacial film mass transfer and intraparticle diffusion, although some consider axial dispersion [4–6].

Melander et al. [7] proposed an eluite–modulator relationship based on some thermodynamic arguments. It can be used for both electrostatic and hydrophobic interactions. In this work, a general rate model for multicomponent elution chromatography [1,8] is used. The model assumes that the eluites follow the multicomponent Langmuir isotherm with a uniform saturation capacity C^{∞}. The adsoption equilibrium constant (b_i) for an eluite is considered to be a function of the modulator concentration observing the eluite–modulator relationship proposed by Melander et al. In this work, the eluites are the human growth hormone (hGH) and an analog of hGH called hGHG120R, which has a potential therapeutic value [9]. The modulator was ACN. The mobile phases in the gradient RP-HPLC were ACN–water solutions with 0.1% (v/v) trifluoroacetic acid (TFA). TFA is commonly used at this concentration to suppress any ion-exchange side effect resulting from the uncapped silanol groups on the RP-HPLC packing.

The gradient rate model is used to predict the column responses of a preparative column based on the eluite–modulator relationship obtained on a small analytical column. Experimental chromatograms are compared with a simulated chromatogram. Parameter estimation and parameter sensitivity analysis for the model are carried out.

2. General rate model for multicomponent gradient elution

The following general rate model was presented by Gu et al. [1]. The model consists of three governing partial differential equations (PDEs), i.e.:

$$-D_{bi}\frac{\partial^2 C_{bi}}{\partial Z^2}+v\frac{\partial C_{bi}}{\partial Z}+\frac{\partial C_{bi}}{\partial t}+\frac{3k_i(1-\epsilon_b)}{\epsilon_b R_p}(C_{bi}-C_{pi,R=R_p})=0 \quad (1)$$

$$(1-\epsilon_p)\frac{\partial C^*_{pi}}{\partial t}+\epsilon_p\frac{\partial C_{pi}}{\partial t}-\epsilon_p D_{pi}\left[\frac{1}{R^2}\frac{\partial}{\partial R}\left(R^2\frac{\partial C_{pi}}{\partial R}\right)\right]=0 \quad (2)$$

$$\frac{\partial C^*_{pi}}{\partial t}=k_{ai}C_{pi}\left(C^{\infty}-\sum_{j=1}^{N_s}C^*_{pi}\right)-k_{di}C^*_{pi} \quad (3)$$

Eqs. (1) and (2) govern the bulk fluid phase and the particle phase, respectively. Eq. (3) is the rate equation for second-order kinetics. The rate constant k_{ai} has units of concentration over time, while the rate constant k_{di} has units of inverse time. If the reaction rates are relatively large compared to the mass transfer rates, then instant adsorption/desorption equilibrium can be assumed, such that both sides of Eq. (3) can be set to zero, which subsequently gives the Langmuir isotherm with the equilibrium constant $b_i=k_{ai}/k_{di}$ for each component,

The PDE system has the following initial and boundary conditions:

$$t=0,\quad C_{bi}=C_{bi}(0,Z), \quad (4)$$

$$t=0,\quad C_{pi}=C_{pi}(0,R,Z) \quad (5)$$

$$z=0,\quad \frac{\partial C_{bi}}{\partial Z}=\frac{v}{D_{bi}}[C_{bi}-C_{fi}(t)] \quad (6)$$

$$Z=L,\quad \frac{\partial C_{bi}}{\partial Z}=0 \quad (7)$$

$$R=0,\quad \frac{\partial C_{pi}}{\partial R}=0 \quad (8)$$

$$R=R_p,\quad \frac{\partial C_{pi}}{\partial R}=\frac{k_i}{\epsilon_p D_{pi}}(C_{bi}-C_{pi,R=R_p}) \tag{9}$$

Defining the dimensionless constants $c_{bi}=C_{bi}/C_{0i}$, $c_{pi}^*=C_{pi}^*/C_{0i}$, $c_{pi}=C_{pi}/C_{0i}$, $\tau=tv/L$, $r=R/R_p$, $z=Z/L$, $Pe_{Li}=vL/D_{bi}$, $Bi_i=k_iR_p/(\epsilon_pD_{pi})$, $\eta_i=\epsilon_pD_{pi}L/(R_p^2v)$, $\xi_i=3Bi_i\eta_i\cdot(1-\epsilon_b)/\epsilon_b$, $Da_i^a=L(k_{ai}C_{0i})/v$, $Da_i^d=Lk_{di}/v$, the model equations can be transformed into the following dimensionless equations:

$$-\frac{1}{Pe_{Li}}\frac{\partial_2 c_{bi}}{\partial z^2}+\frac{\partial c_{bi}}{\partial z}+\frac{\partial c_{bi}}{\partial \tau}+\xi_i(c_{bi}-c_{pi,r=1})=0 \tag{10}$$

$$\frac{\partial}{\partial \tau}[(1-\epsilon_p)c_{pi}^*+\epsilon_p c_{pi}]-\eta_i\left[\frac{1}{r^2}\frac{\partial}{\partial r}\left(r^2\frac{\partial c_{pi}}{\partial r}\right)\right]=0 \tag{11}$$

$$\frac{\partial c_{pi}^*}{\partial \tau}=Da_i^a c_{pi}\left(c_i^\infty-\sum_{j=1}^{N_s}\frac{C_{0j}}{C_{0i}}c_{pj}^*\right)-Da_i^d c_{pi}^* \tag{12}$$

If the saturation capacities are the same for all the components, at equilibrium, Eq. (12) gives $b_iC_{0i}=Da_i^a/Da_i^d$ and $a_i=C^\infty b_i=c_i^\infty Da_i^a/Da_i^d$ for the resultant multicomponent Langmuir isotherm below:

$$C_{pi}^*=\frac{a_iC_{pi}}{1+\sum_{j=1}^{N_s}b_jC_{pj}}$$

or

$$c_{pi}^*=\frac{a_ic_{pi}}{1+\sum_{j=1}^{N_s}(b_jC_{0j})c_{pj}}$$

(dimensionless) (13)

The dimensionless initial and boundary conditions are listed below.

Initial conditions:

$$\tau=0,\quad c_{bi}=c_{bi}(0,z)\quad c_{pi}=c_{pi}(0,r,z) \tag{14}$$

Boundary conditions:

At $r=0$

$$\partial c_{pi}/\partial r=0 \tag{15a}$$

and at $r=1$

$$\partial c_{pi}/\partial r=Bi_i(c_{bi}-c_{pi,r=1}) \tag{15b}$$

$$z=0,\quad \partial c_{bi}/\partial z=Pe_{Li}[c_{bi}-C_{fi}(\tau)/C_{0i}] \tag{16}$$

The modulator is designated as the last component in a multicomponent system, which is component N_s. Thus, the eluite–modulator relationship proposed by Melander et al. [7] can be written as follows:

$$\log_{10}b_i=\alpha_i-\beta_i\log_{10}C_{p,N_s}+\gamma_iC_{p,N_s} \tag{17}$$

in which α_i, β_i and γ_i are experimental correlation parameters. Note that Melander et al. used the retention factor k_i' (also known as the capacity factor) instead of b_i in their proposed eluite–modulator relationship. k_i' and b_i are, however, related.

The retention factor is defined by Snyder and Kirkland [10] as the ratio of the total moles of a component in the stationary phase to that in the mobile phase. It is easy to show that for an isocratic elution with a dilute sample (containing component i) which observes the linear range of the Langmuir isotherm, we have $k_i'=\phi C^\infty b_i$. ϕ is the phase ratio (particle skeleton volume to mobile-phase volume including the particle macropores inside the column), which can be determined from the bed void fraction and particle porosity as follows:

$$\phi=(1-\epsilon_b)(1-\epsilon_p)/[\epsilon_b+(1-\epsilon_b)\epsilon_p] \tag{18}$$

ϕC^∞ is a constant, and can be separated from $\phi C^\infty b_i$ and lumped into the α_i term in Eq. (17). Thus, Eq. (17) yields:

$$\log_{10}k_i'=\alpha_i'-\beta_i\log_{10}C_m+\gamma_iC_m \tag{19}$$

where $\alpha_i'=\alpha_i+\log_{10}\phi C^\infty$, i.e. $\alpha_i=\alpha_i'-\log_{10}\phi C^\infty$, and C_m is the modulator concentration. In the model system, $C_m=C_{p,N_s}$ in Eq. (11). Because the modulator is non-binding, Eqs. (10) and (11) are linear for the modulator (i.e. component N_s). C_m can have units other than mole l^{-1}, while other binding components must have units of mol l^{-1} in order to be consistent with C^∞. For convenience, the volume fraction was adopted for C_m in this work.

It is assumed that eluites do not interfere with each other's correlation parameters in Eq. (17).

The saturation capacities for all eluites are the same, and they are not affected by the modulator concentration.

For gradient elution, the model requires the following initial conditions: at $\tau=0$, $C_{bi}=c_{pi}=c_{pi}^{*}=0$ for the eluites ($i=1, 2, \ldots, N_s-1$), and at $\tau=0$, $c_{bi}=c_{pi}=C_{m0}/C_{0i}=c_{m0}$ and $c_{pi}^{*}=0$ for the modulator ($i=N_s$). The following boundary condition describes a sample injection in the form of a rectangular pulse for the eluites ($i=1, 2, \ldots, N_s-1$):

$$C_{fi}(\tau)/C_{0i}=\begin{cases}1 & 0\le\tau\le\tau_{imp}\\ 0 & \tau>\tau_{imp}\end{cases} \quad (20)$$

The upper boundary value of the rectangular sample pulse of an eluite is taken as its reference concentration value C_{0i}. In the model, $\tau=0$ corresponds to the moment when the sample starts to enter the column. In reality, the chromatogram recorder starts recording when the sample starts to leave the sample loop. The volume space between the sample loop and the column inlet is usually negligible. Thus, time zero on the experimental recorded chromatogram maybe considered $\tau=0$ in the model.

τ_{imp} is the dimensionless time it takes to pump the sample. If the sample volume is V_{imp}, and the mobile phase volumetric flow rate is Q, then:

$$\tau_{imp}=t_{imp}(v/L)=(V_{imp}/Q)v/L=V_{imp}/(V_b\epsilon_b) \quad (21)$$

in which V_b is the bed volume of the column, and v is the interstitial velocity of the mobile phase. v is calculated using the following relationship based on its definition:

$$v=QL/(V_b\epsilon_b) \quad (22)$$

The boundary condition for the modulator ($i=N_s$) at the column inlet can take the following general form:

$$C_{fi}(\tau)/C_{0i}\begin{cases}=C_{m0}/C_{0i} & \tau\le\tau_{imp}\\ \ge(\text{or}\le)C_{m0}/C_{0i} & \tau>\tau_{imp}\end{cases} \quad (23)$$

In this work, C_m has units of the volume fraction of ACN, and C_{0i} (with $i=N_s$) was set to unity for ACN. Thus, $C_{m0}/C_{0i}=C_{m0}=$the volume fraction of ACN in the mobile phase which is used to equilibrate the column before sample injection. After sample injection, the mobile-phase feed can take any value depending on the kind of gradient profile used for elution. In this work, only a linear gradient was used. Thus, the gradient profile can be described by the following function:

$$C_{fi}(\tau)/C_{0i}=\begin{cases}C_{m0} & \tau\le\tau_{delay}\\ a_1+a_2(\tau-\tau_{imp}) & \tau>\tau_{delay}\end{cases} \quad (24)$$

where $a_1=C_{m0}-a_2(\tau_{delay}-\tau_{imp})$, and $a_2=\Delta C_m/\Delta\tau$. a_2 is the dimensionless gradient slope, $\Delta\tau$ is the dimensionless gradient time duration, and τ_{delay} is the dimensionless time it takes for the gradient front to reach the column inlet. In an ideal situation, the gradient front is initially at the end of the sample stream, and thus $\tau_{delay}=\tau_{imp}$ and $a_1=C_{m0}$. In reality, the gradient front forms first at the gradient mixer. The sample may occupy only a portion of the sample loop near the column inlet. τ_{delay} is the dimensionless time for the gradient front to travel through the sample loop to the column inlet if the fluid volume between the gradient mixer and the end of the sample loop is ignored. Thus:

$$\tau_{delay}=\tau_{delay}(v/L)=(V_{loop}/Q)v/L=V_{loop}/(V_b\epsilon_b) \quad (25)$$

where V_{loop} is the volume of the sample loop.

3. Numerical method

The model was solved [1,8] numerically with a FORTRAN 77 code. The finite element method (with quadratic elements) and the orthogonal collocation method were used to discretize the bulk-fluid phase and the particle-phase PDEs, respectively. The resulting ODEs together with Eq. (12) were solved using the public-domain ODE solver called DVODE of Brown et al. [11]. All the simulation in this work was carried out on a Pentium 150 MHz personal computer (PC) with the Windows 95 operating system.

Because the asymptotic limit of the kinetic model is the equilibrium rate model, the kinetic model can easily be converted into an equilibrium rate model for gradient elution. One only has to set the Damköhler number for the desorption (or

adsorption) of eluites ($i=1, 2, \ldots, N_s-1$) in the kinetic model to a large arbitrary value (say, no less than 1000) and then calculate the Damköhler number for adsorption (or desorption) from the relationship $Da_i^a/Da_i^d = b_i C_{0i}$, where b_i is obtained from Eq. (17). By doing so, Eq. (17) is combined with the kinetic model without any difficulty. The incorporation of initial conditions into the FORTRAN code required for gradient elution is straightforward.

4. Parameter estimation

4.1. Bed void fraction and particle porosity

According to Unger [12], for a typical column packed with 5 μm silica-based particles, the bed void fraction $\epsilon_b=0.4$. The particle porosity can be calculated from the following relationship:

$$\epsilon_{total} = \epsilon_b + (1-\epsilon_b)\epsilon_p \quad (26)$$

where the total voidage ϵ_{total} is obtained from the dead volume time for unretained small molecules (such as salts and solvents) t_0. In RP-HPLC, the retention time of the solvent front may be taken as t_0. Thus:

$$\epsilon_{total} = Qt_0/V_b \quad (27)$$

where Q is the volumetric flow rate of the mobile phase, and V_b is the bed volume of the column. Combining Eqs. (26) and (27), we have:

$$\epsilon_p = (Qt_0/V_b - \epsilon_b)/(1-\epsilon_b) \quad (28)$$

ϵ_p can be measured more accurately using a mercury porosimeter. If so, Eq. (28) can be used to calculate ϵ_b without using Unger's value of 0.4. ϵ_b can also be evaluated using the standard blue dextrin method.

4.2. Adsorption saturation capacity

The adsorption saturation capacity (C^∞) is defined as the maximum molar amount of the eluite adsorbed onto the stationary phase per unit volume of the particle skeleton. It is the leveling-off limit in the Langmuir isotherm. C^∞ can be obtained using the method introduced by Snyder and Stadalius [13]. The method is based on the small retention time difference (Δt_R) between two gradient runs, one with a small sample and the other with a large sample. The following equation is given by Snyder et al. [14]:

$$w_s = 4pw_x/(1-10^{-\Delta t_R G/t_0})^2 \quad (29)$$

where w_s is defined as the column saturation capacity (mg of eluite) corresponding to a very concentrated equilibrium concentration. p is an empirical parameter with a value of 5/8. w_x is the amount of eluite (mg) in the large sample. w_x should be sufficiently large such that the Δt_R is large enough to be measured. G is the gradient steepness parameter, which is calculated from [14]:

$$G = V_m \Delta C_m S/(t_G Q) \quad (30)$$

where V_m is the total void volume in the column, which is equal to Qt_0, and ΔC_m is the change in volume fraction of the organic modifier (ACN in this work) during the gradient. t_G is the gradient time, and S is a parameter originating from isocratic elution. It is defined as $S = d(\log_{10} k)/dC_m$. For proteins within the molecular-weight range $600 \le M \le 80\,000$, Snyder and Stadalius [13] suggested the following simple correlation:

$$S = 0.48M^{0.44} \quad (31)$$

Combining Eq. (29) and Eq. (30), w_s can be calculated using the following equation:

$$w_s = 2.5w_x/(1-10^{-0.48M^{0.44}\Delta t_R \Delta C_m/t_G})^2 \quad (32)$$

The adsorption saturation capacity (C^∞) can be derived directly from w_s using the following relationship based on the definition of C^∞:

$$C^\infty = w_s/[MV_b(1-\epsilon_b)(1-\epsilon_p)] \quad (33)$$

C^∞ can also be calculated using the standard batch adsorption method if packing particles are available separately.

4.3. Eluite–modulator relationship

The capacity factor (k') of an eluite at a fixed mobile-phase concentration (C_m) can be evaluated with a single isocratic run. According to Snyder

and Kirkland [10]:

$$k' = (t_R - t_0)/t_0 \quad (34)$$

If several isocratic runs are performed with different mobile-phase concentrations, a plot of k' versus C_m can be obtained. The data points can be correlated to obtain the correlation parameters α_i, β_i and γ_i in Eq. (19).

4.4. Dimensionless mass transfer parameters Pe, η, and Bi for individual components

These three parameters can all be estimated using existing correlations in the literature. Because the rate model is not very sensitive to the three parameters, when the their values are sufficiently large, further increase will only slightly sharpen a peak [8]. Thus, there is no need to obtain their values experimentally.

The Peclet number can be evaluated from the experimental correlation by Chung and Wen [15], i.e.:

$$Pe = [L/(2R_p\epsilon_b)](0.2 + 0.011Re^{0.48})$$
$$0.001 < Re < 1000 \quad (35)$$

where L is the column length and R_p is the particle radius. Usually, the Reynolds number, $Re = \epsilon_b v \rho_f (2R_p)/\mu_f$, for a liquid chromatography column is very small, such that the Re term in the expression above can be ignored. Thus, we have:

$$Pe = 0.1L/(R_p\epsilon_b) \quad (36)$$

The evaluation of $\eta = \epsilon_p D_p L/(R_p^2 v)$ requires the value of the effective intraparticle diffusivity D_p. D_p can be calculated from the molecular diffusivity from a correlation by Yau et al. [16], i.e.:

$$D_p = D_m(1 - 2.104\lambda + 2.09\lambda^3 - 0.95\lambda^5)/\tau_{tor} \quad (37)$$

in which $\lambda = d_m/d_p$, i.e. the ratio of the molecular diameter of the eluite to the pore diameter of the particles. The particle tortuosity factor τ_{tor} varies from about 1.5 to over 10 [17]. A reasonable range for many commercial porous solids is about 2–6 [17,18]. For the 5 μm particle used in this work, $d_p = 300$ Å according to the specifications from the column vendor. Marshall [19] suggested that the average specific volume for proteins is in a narrow range of 0.728–0.751 $cm^3\ g^{-1}$. He also recommended 0.2 g water per g protein as a typical hydration rate. If a hydrated protein is considered spherical and its specific volume is 0.7384 $cm^3\ g^{-1}$, the following empirical relationship between the molecular weight and the hydrodynamic diameter exists:

$$d_m(\text{Å}) = 2[3MV_{s,h}/(4\pi 6.02 \times 10^{23})]^{1/3} = 1.44M^{1/3} \quad (38)$$

where the hydrated specific volume is calculated [20] from $V_{s,h} = 0.7384\ cm^3\ g^{-1} + (0.2$ g water per g protein$) \times (1\ cm^3\ g^{-1}$ water). D_m can also be estimated directly from the molecular weight. Polson [21] obtained a semiempirical relationship for organic substances (including proteins) with a molecular weight greater than 1000, i.e.:

$$D_m(cm^2\ s^{-1}) = 2.74 \times 10^{-5} M^{-1/3} \quad (39)$$

The interstitial velocity is calculated from Eq. (22). With the values of ϵ_p, D_p, L, V_b, and v known, $\eta = \epsilon_p D_p L/(R_p^2 v)$ can be calculated.

The evaluation of the Biot number $Bi = kR_p/(\epsilon_p D_p)$ requires the value of the film mass transfer coefficient k. k can be obtained from a correlation by Wilson and Geankoplis [22,23], i.e.:

$$Sh = 1.09(ReSc)^{1/3}/\epsilon_b = 1.37(v\epsilon_b R_p/D_m)^{1/3}/\epsilon_b$$
$$(0.0015 < Re < 55) \quad (40)$$

in which the Sherwood number $Sh = k(2R_p)/D_m$, and the Schmidt number $Sc = \mu_f/(\rho_f D_m)$. The product $v\epsilon_b$ is the superficial velocity. The applicable range of the Reynolds number covers liquid chromatography. Eq. (40) can be easily rearranged to yield:

$$k = 0.687v^{1/3}(\epsilon_b R_p/D_m)^{-2/3} \quad (42)$$

The k values can also be calculated from an experimental correlation obtained by Kataoka et al. [24] for an ion-exchange resin, i.e.:

$$k/v = 1.85[\epsilon_b/(1-\epsilon_b)]^{1/3}(Re'Sc)^{-2/3} \quad (Re' < 100) \quad (43)$$

in which the modified Reynolds number is defined as $Re' = (v\epsilon_b)(2R_p)\rho/[\mu(1-\epsilon_b)]$. Eq. (43) can be

rearranged to give:

$$k = 1.165[v(D_m/R_p)^2(1-\epsilon_b)/\epsilon_b]^{1/3} \quad (44)$$

Multiplying $0.589[(1-\epsilon_b)\epsilon_b]^{-1/3}$ with the right-hand side of Eq. (44) gives the right-hand side of Eq. (42). This value is within $\pm 8.5\%$ of unity for $0.2 < \epsilon_b < 0.8$. This means the two correlations are very close. In this work, $\epsilon_b = 0.4$. The k values calculated from Eq. (44) were only 5.2% larger than those calculated from Eq. (42). Eq. (42) was used in this work to calculate k.

5. Experimental

A Waters (Millipore Corp., Bedford, MA) dual-pump gradient HPLC system was used for the analysis of protein concentrations. This computer-controlled system had two Model 510 pumps, a Model U6K detector with a 2.5 ml sample loop, and a Model 486 UV detector. The computer software was Waters' BASELINE 810 package. A Waters 600E quaternary preparative gradient pump was used when a large sample was involved. Two reversed-phase HPLC columns were used. Both were Vydac brand columns from the Separations Group (Hesperia, CA). They had the same packing material, which was C4 with a particle size of 5 μm and a pore size of 300 Å. One of the columns was a small analytical column with dimensions of 25 cm × 4.6 mm i.d. (Vydac 214 TP54). Its bed volume was 4.15 ml. The other column was a 25 cm × 10 mm i.d. preparative column (Vydac 214TP510) with a bed volume of 19.63 ml.

The mobile phase consisted of HPLC-grade ACN, deionized water and TFA. The TFA concentration in the mobile phase was 0.1% (v/v) in all experiments. In RP-HPLC, TFA causes the baseline to shift slightly upward. This upward shift is amplified when the UV absorbance scale is small. This phenomenon is because TFA's absorbance increases slightly following the increase of ACN in a gradient. The presence of TFA was ignored in our simulation. Human growth hormone (hGH) and a recombinant human growth hormone analog named hGHG120R [9] were used as proteins. They differ by only one amino acid among 191 amino acids: namely, hGHG120R has arginine (R) at position 120, while hGH has glycine (G).

6. Results and discussion

On the small analytical column, three isocratic runs with three different ACN concentrations (56.99, 61.83 and 65.02%, respectively) were carried out for hGH. Similar runs were performed for hGHG120R. Fig. 1 was obtained by plotting the experimental results of the retention factors of hGH and hGHG120R at the three ACN concentrations. Fig. 1 indicates that hGH binds more strongly with the stationary phase of the column than hGHG120R. The two straight lines in Fig. 1 yielded the α_i', β_i and γ_i data in Table 1. The semi-log linear behavior in Fig. 1 is consistent with observations made by Horvath and coworkers [4,7].

To obtain the adsorption saturation capacity, two runs were carried out using hGHG120R with a 30 min gradient from 40% ACN + 0.1% TFA to 80% ACN + 0.1% TFA at a flow rate of 1 ml min^{-1} on the analytical column. The first run used a small sample and the second run used a relatively large sample containing $w_x = 2.176$ mg of HGHG120R. The two retention times were 22.50

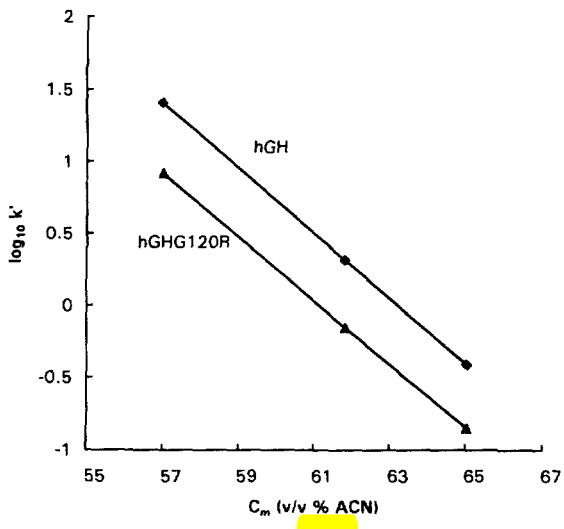

Fig. 1. Capacity factor versus acetonitrile concentration for hGH and hGHG120R.

Table 1
Eluite–modulator retention relationship

Protein	C^{∞} (mol l^{-1})	ϕ	α_i'	$\alpha_i=\alpha_i'-\log_{10}\phi C^{\infty}$	β_i	γ_i
hGHG120R	2.2×10^{-4}	0.495	13.6875	17.650	0	−22.3863
hGH	2.2×10^{-4}	0.495	14.4935	18.456	0	−22.9190

and 20.48 min, respectively. Thus, the retention time difference is $\Delta t_R=2.02$ min. Inserting $w_x=2.176$ mg, $\Delta t_R=2.02$ min, $M=22\,000$, $\Delta C_m=0.4$ and $t_G=30$ min into Eq. (32), it is calculated that $w_s=6.55$ mg. w_s is converted into the adsorption saturation capacity (C^{∞}) using Eq. (33), which gives $C^{\infty}=2.2\times10^{-4}$ mol l^{-1} for hGHG120R. It was assumed that hGH had the same C^{∞} value in this work.

The solvent time for the analytical column was found to be 2.78 min with a flow rate of 1 ml min^{-1} in an experimental chromatogram. With this information, the particle porosity was calculated using Eq. (28) with $\epsilon_b=0.4$ to give a value of $\epsilon_p=0.45$. The phase ratio ϕ was found to be 0.495 based on Eq. (18).

Fig. 2(A) is the experimental chromatogram for a gradient run with a 40 μl hGHG120R sample. The sample concentration was 5.5×10^{-6} mol l^{-1}. The gradient was 40% ACN+0.1% TFA to 80% ACN+0.1% TFA in 30 min at 1 ml min^{-1}. Fig. 2(B) is the simulated chromatogram. The data used for the simulation are listed in Table 2. A particle tortuosity of $\tau_{tor}=4$ was used for simulated peaks in all the figures in this work. τ_{tor} was found to be insensitive in this work. For the parameters used to obtain Fig. 2(B), the dimensionless peak heights were 0.106, 0.103, 0.100 and 0.097 for τ_{tor} values of 2, 4, 6 and 8, respectively. Such small variations in peak heights hardly affect the peak width for such a sharp peak in Fig. 2(B) since the peak areas must be the same due to mass balance. When τ_{tor} increases, *Bi* increases and η decreases proportionally. For large *Bi* values (say $Bi>50$), the interior collocation number must sometimes be set to 3, otherwise numerical integration fails. This is because intraparticle diffusion is very dominant for large *Bi* values. The insensitivity of τ_{tor} in this work is not universal. For example, in size exclusion chromatography, τ_{tor} has a significant impact on peak widths [25].

From Table 2 it can be seen that the raw data used for parameter estimation are not difficult to obtain. In Fig. 2, the experimental and simulation retention times are 22.5 and 21.6 min, respectively. The simulated peak width is also close to the actual peak width. A peak height comparison was not performed, since it is not an important factor in the model prediction. The simulated effluent profile of ACN is shown in Fig. 2(B).

The Peclet number, η number and Biot number listed in Table 2 for ACN are very large, and they overburden numerical calculations. It turns out that they could be artificailly set to much smaller values without showing any visual difference in ACN's effluent profiles, as indicated by Fig. 3. This is because the ACN effluent profile is not a peak, but a rather flat gradient profile. Fig. 3 shows that the Peclet number, η number and Biot number need not be estimated for ACN at all. They can be artificially set to 500, 5 and 5, respectively, for convenience without contributing any detectable simulation error for eluite peaks.

Fig. 4 shows the experimental and simulated chromatograms for a binary elution on the Vydac preparative column using a sample containing 5.7×10^{-7} mol l^{-1} of hGH and 5.5×10^{-6} mol l^{-1} of hGHG120R with a gradient of 40% ACN+0.1% TFA to 80% ACN+0.1% TFA in 30 min at 2 ml min^{-1}. The sample volume was 40 μl. The dimensionless peak height of hGH was comparable to that of hGHG120R because of the nature of dimensionless concentration. In order to have a better visual comparison, the dimensionless concentration of hGH was scaled down by a factor of 10 in the simulated chromatogram since its feed concentration was about one tenth that of hGHG120R. Simulation parameters are listed in

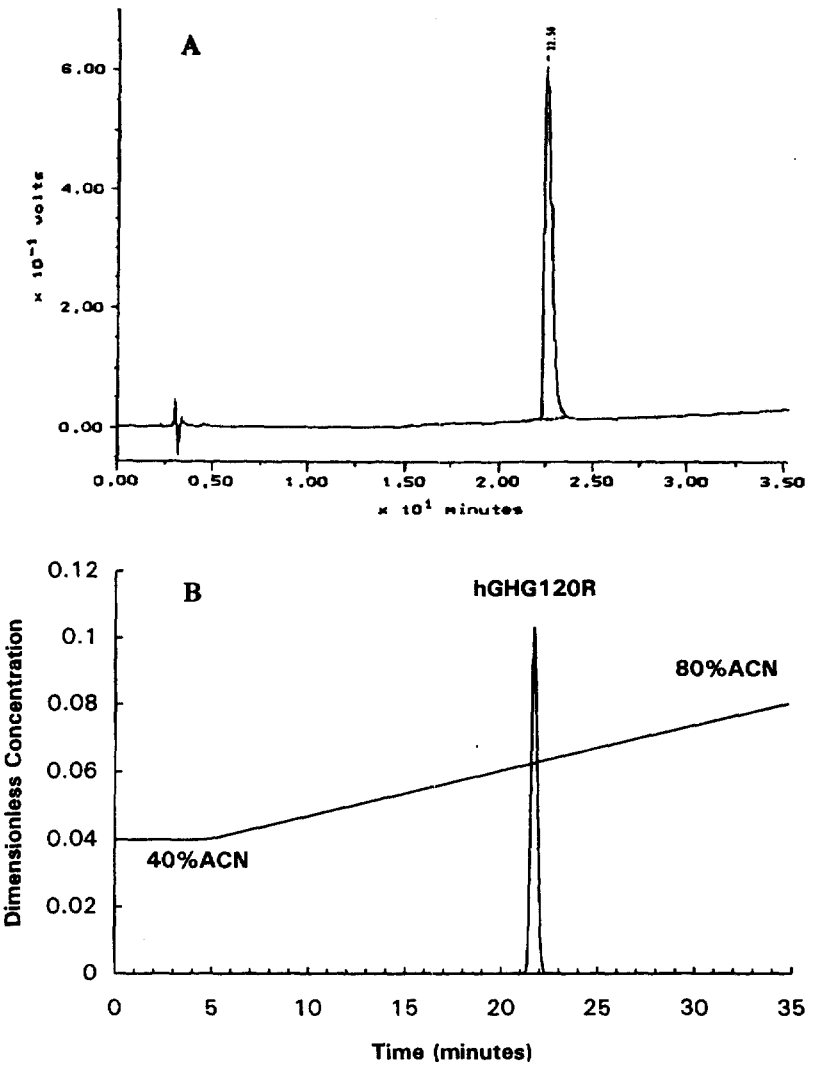

Fig. 2. Experimental and simulted chromatograms for hGHG120R on the analytical column.

Table 3. The eluite–modulator retention relationship and the ϵ_p value obtained from the analytical column were used for the simulation. No a posteriori operational data from the preparative column were needed.

The recalculation of simulation parameters for a new simulation run is quite convenient if one uses a spreadsheet software program such as Microsoft© Excel. The updated parameters can be generated automatically by the built-in formulae in the spreadsheet.

Fig. 5 shows the experimental and simulated chromatograms for a small hGHG120R sample on the Vydac preparative column using a 40 μl sample containing 8.8×10^{-6} mol l^{-1} of hGHG120R with a gradient of 40% ACN + 0.1% TFA to 80% ACN + 0.1% TFA in 40 min at 2 ml min^{-1}. Fig. 6 shows a comparison of experimental and simulated chromatograms for a gradient elution involving a large sample on the preparative Vydac column using the Waters 600E quaternary preparative gradient pump. In the experimental chromatogram, the flat top of the hGHG120R peak indicates that the peak concen-

Table 2
Parameters used for Fig. 2(B)[a]

Direct raw data			
V_{imp} (sample size, ml)	40×10^{-3}		
C_{sample} (sample concentration, mol l^{-1})	5.5×10^{-6}		
ΔC_m (ACN volume fraction difference)	0.4 ($=C_{m,end}-C_{m0}=80\%-40\%$)		
t_G (gradient time, min)	30		
Q (flow rate, ml min^{-1})	1		
L (column length, cm)	25		
d_c (column diameter, cm)	0.46		
t_0 (solvent time, min)	2.78		See Fig. 2(A)
V_{loop} (sample loop size, ml)	2		
R_p (particle radius, cm)	2.5×10^{-4}		
ϵ_b (bed voidage)	0.4		
τ_{tor} (tortuosity)	4		
d_p (pore diameter, Å)	300		
Calculated data			
V_b ($=\pi d_c^2 L/4$, bed volume, ml)	4.155		
v (interstitial velocity, cm s^{-1})	0.251		Eq. (22)
ϵ_p (particle porosity)	0.45		Eq. (28)
τ_{imp} (dimensionless injection time)	0.0241		Eq. (21)
τ_{delay} (dimensionless delay time)	1.203		Eq. (25)
$a_1 = C_{m0} - a_2(\tau_{delay} - \tau_{imp})$	0.3739		Eq. (24)
$a_2 = \Delta C_m/\Delta\tau = \Delta C_m/(t_G v/L)$	0.02216		Eq. (24)
	hGHG120R	ACN	
d_m (molecular diameter, Å)	40.35	4.97	Eq. (38)
$\lambda = d_m/d_p$	0.1345	0.0166	
D_m (molecular diffusivity, $cm^2\ s^{-1}$)	9.78×10^{-7}	3.41×10^{-6}	Eq. (39)
D_p (effective, intraparticle diffusivity, $cm^2\ s^{-1}$)	1.77×10^{-7}	1.92×10^{-6}	Eq. (37)
k (film mass transfer coefficient, cm s^{-1})	0.0198	0.0800	Eq. (42)
Pe_L (Peclet number)	25 000	25 000	Eq. (36)
$\eta = \epsilon_p D_p L/(R_p^2 v)$	126.3	1370	
$Bi = kR_p/(\epsilon_p D_p)$, Biot number	62.54	23.28	
L/v (min)	1.662		

[a]The computer code requires the following parameters as data input: N (=2, number of components), N_e (number of finite elements, set to 21), N_c (number of interior collocation points, set to 3), τ_{imp}, ϵ_p, ϵ_b, Pe_{Li}, η_i, Bi_i, C_{0i} (set to 100% for ACN; = C_{sample} for protein), C^∞, α_i, β_i, γ_i, C_{m0}, τ_{delay}, a_1, and a_2. The L/v value is needed to convert τ into real time. C^∞, α_i, β_i and γ_i values are listed in Table 1.

tration is out of the UV response range. In the experiment, 50 ml hGHG120R with a concentration of 8.8×10^{-6} mol l^{-1} was pumped into the column without using the injector due to the large size of the sample. Before the gradient was started, 120 ml of 40% ACN + 0.1% TFA was used to wash the column. Subsequently, a gradient of 40% ACN to 80% ACN in 60 min at 2 ml min^{-1} was used to elute the hGHG120R peak out.

The parameters related to Fig. 6(B) are listed in Table 4. The gradient delay volume (174 ml) was calculated by adding the sample volume (50 ml), the wash volume (120 ml) and the volume between the gradient mixer and the column inlet, which was 4 ml. The gradient delay volume indicates that there were 174 ml of 40% ACN + 0.1% TFA between the head of the sample stream and the gradient front. Time zero in simulation was the moment when the sample entered the column inlet. Due to the long length of the actual chromatograhic run, in the experimental chromatogram recording was started when the gradient was set to go from the gradient mixer, unlike other cases in which recording was started at the moment

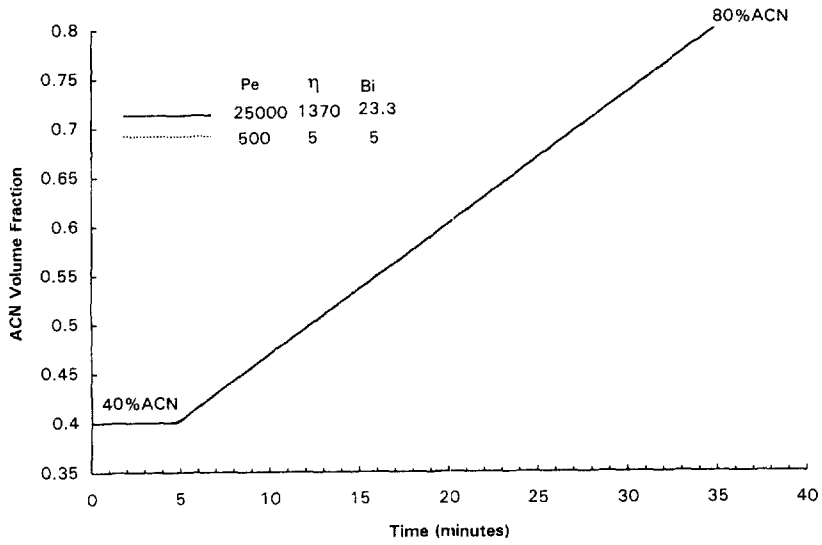

Fig. 3. Effect of mass transfer parameters on acetonitrile gradient profile.

when the sample was first introduced. This means recording was started after a total of 170 ml (i.e. 50 ml sample + 120 ml wash) liquid had been pumped in. At a flow rate of 2 ml min^{-1}, this means that recording was started 85 min later than usual. In order to compare the time in the experimental chromatogram and the time in the simulated chromatogram, the following formula was used to convert dimensionless τ in the simulation into the time t (min) used in the experimental chromatogram:

$$t = \tau/(v/L) - t_{adj} \quad (45)$$

where $t_{adj} = 85$ min. For Fig. 6, $\eta = 299.46$ and $Bi = 46.8$ were too stiff numerically. They were reset to $\eta = 10$ and $Bi = 10$ to give the solid-line peak. The two almost indistinguishable dashed-line peaks in Fig. 6 were calculated with $\eta = 20$, $Bi = 20$ and $\eta = 40$, $Bi = 40$, respectively. Obviously, further increasing the η and Bi values would only make the case computationally more time-consuming, while not causing any significant change in the peak profile. This case was very stiff, because the very large sample load took a long time to diffuse inside the column during migration, thus drastically prolonging the stiffness in numerical integration during simulation.

Fig. 7 shows the effect of the C^{∞} value on gradient profiles. All simulation input data are the same as in Fig. 2 except C^{∞}. Fig. 7 shows that the peak retention time and profiles are not very sensitive to the change in C^{∞} for gradient elutions in reversed-phase chromatography. In this case, the deviation of the C^{∞} value by 100% results in a retention-time difference of about 1 min. This means that C^{∞} does not need to be estimated with a very high accuracy. If the target protein is expensive, a less expensive similar protein may be used instead to measure C^{∞}.

The Peclet numbers for proteins in all cases were 25 000, based on Eq. (36). This large Peclet number caused unnecessary difficulties in numerical calculation, and thus the Peclet numbers for proteins were set to 1000 for all simulations in this work. Fig. 8 shows the effect of the Peclet number on the protein peak profile. In Fig. 8, the solid-line peak has the same parameters as Fig. 2(B). Apparently, the Peclet number affects peak height, but its effect on peak width is very limited when its value is 1000 and above. This is common for fixed-bed problems.

The sensitivities of ϵ_b and ϵ_p were studied by recalculating Fig. 2(B) using ϵ_b values of 0.3 and 0.45. From Eq. (28) with fixed Q, t_0 and V_b values, the recalculated ϵ_p values were 0.53 and 0.4, respectively. C^{∞} changed very little, based on Eq. (33).

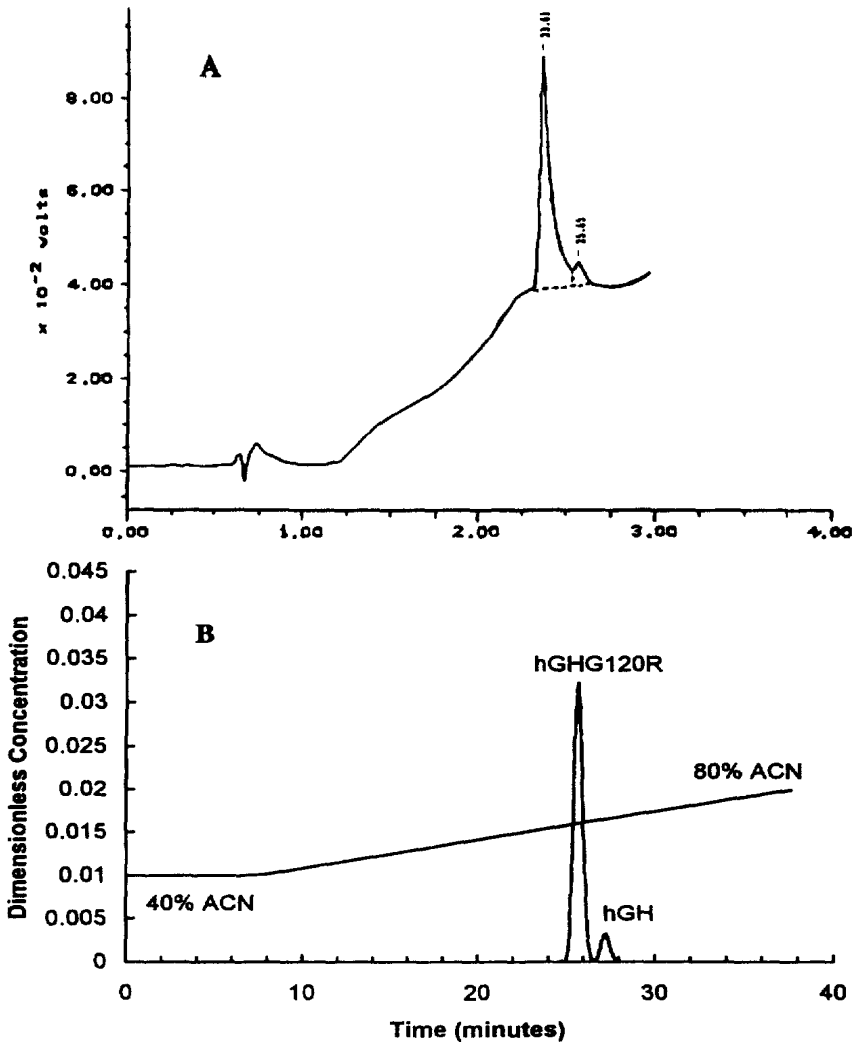

Fig. 4. Experimental and simulated chromatograms for a binary protein sample on the preparative column.

Numerical simulations showed that for $\epsilon_b = 0.3$, 0.4 and 0.45, there was no retention-time change, and the corresponding dimensionless peak heights were 0.106, 0.102 and 0.103, respectively. Thus, there was hardly any change in peak width in the given scenario.

The parameters α and γ in the eluite–modulator relationship of Eq. (17) were found to be very sensitive. The middle peak in Fig. 9 is the same as that in Fig. 2(B). The other four peaks were calculated after varying α or β by 10%. The three solid-line peaks in Fig. 9 indicate that increasing γ (corresponding to the stiffer hGHG120R line in Fig. 1) will reduce the peak retention time and sharpen the peak. The two dashed-line peaks and the middle peak in Fig. 9 show that increasing α (i.e. moving up the hGHG120R line in Fig. 1) will increase the peak retention time without changing the peak height.

All the simulated chromatograms in this work were calculated on a Pentium 150 MHz PC with 32 MB RAM. The executable program was compiled from a FORTRAN 77 source code using Microsoft Fortran PowerStation 4.0 (for Windows

Table 3
Parameters used for Fig. 4(B)[a]

Direct raw data		
V_{imp} (sample size, ml)	40×10^{-3}	
C_{sample} (sample concentration, mol l^{-1})	5.5×10^{-7} for hGH and 5.5×10^{-6} for hGHG120R	
ΔC_m (ACN volume fraction difference)	0.4 ($= C_{m,end} - C_{m0} = 80\% - 40\%$)	
t_G (gradient time, min)	30	
Q (flow rate, ml min^{-1})	2	
L (column length, cm)	25	
d_c (column diameter, cm)	1	
t_0 (solvent time, min)	2.78	See Fig. 2(A)
V_{loop} (sample loop size, ml)	2	
R_p (particle radius, cm)	2.5×10^{-4}	
τ_{tor} (tortuosity)	4	
d_p (pore diameter, Å)	300	
ϵ_b (bed voidage)	0.4	
Calculated data		
V_b ($= \pi d_c^2 L/4$,, bed volume, ml)	19.63	
v (interstitial velocity, cm s^{-1})	0.106	Eq. (22)
τ_{imp} (dimensionless injection time)	5.09×10^{-3}	Eq. (21)
ϵ_p (particle porosity)	0.45	
τ_{delay} (dimensionless delay time)	0.2546	Eq. (25)
$a_1 = C_{m0} - a_2(\tau_{delay} - \tau_{imp})$	0.38694	Eq. (24)
$a_2 = \Delta C_m/\Delta\tau = \Delta C_m/(t_G v/L)$	0.05236	Eq. (24)
	hGHG120R	
d_m (molecular diameter, Å)	40.35	Eq. (38)
$\lambda = d_m/d_p$	0.1345	
D_m (molecular diffusivity, $cm^2\ s^{-1}$)	9.78×10^{-7}	Eq. (39)
D_p (effect, intraparticle diffusivity, $cm^2\ s^{-1}$)	1.77×10^{-7}	Eq. (37)
k (film mass transfer coefficient, cm s^{-1})	0.0148	Eq. (42)
Pe_L (Peclet number)	25 000	Eq. (36)
$\eta = \epsilon_p D_p L/(R_p^2 v)$	299.5	
$Bi = kR_p/(\epsilon_p D_p)$, Biot number	46.8	
L/v (min)	3.928	

[a]The computer code requires the following parameters as data input: N (=3, number of components), N_e (number of finite elements, set to 25), N_c (number of interior collocation points, set to 2), τ_{imp}, ϵ_p, ϵ_b, Pe_{Li}, η_i, Bi_i, C_{0i} (set to 100% for ACN; = C_{sample} for protein), C^∞, α_i, β_i, γ_i, C_{m0}, τ_{delay}, a_1 and a_2. The L/v value is needed to convert τ into real time. The values of C^∞, α_i, β_i and γ_i are listed in Table 1.

95). The calculation times were in the range of several minutes to tens of minutes. Previously [1], the FORTRAN source code (for Unix computers) used a commercial ODE solver, i.e. IVPAG from the International Mathematical and Statistical Library (IMSL). The PC version used in this work adopts the public-domain ODE solver called DVODE, written by Brown et al. [10]. Multiple runs can be carried out simultaneously on a PC. The binary executable can be ported to any PC running Windows 95 with a minimum of 8 MB RAM. The binary executables for both Windows 95 and MS-DOS platforms are available free of charge from the corresponding author of this work for noncommercial applications. Information on how to obtain them and other related chromatographic simulation packages can be found at http://www.ent.ohiou.edu/~guting/ on the World Wide Web. They can also be obtained by sending an e-mail to gu@ohiou.edu.

7. Conclusions

This work shows that the rate model system predicts the retention time and peak width for

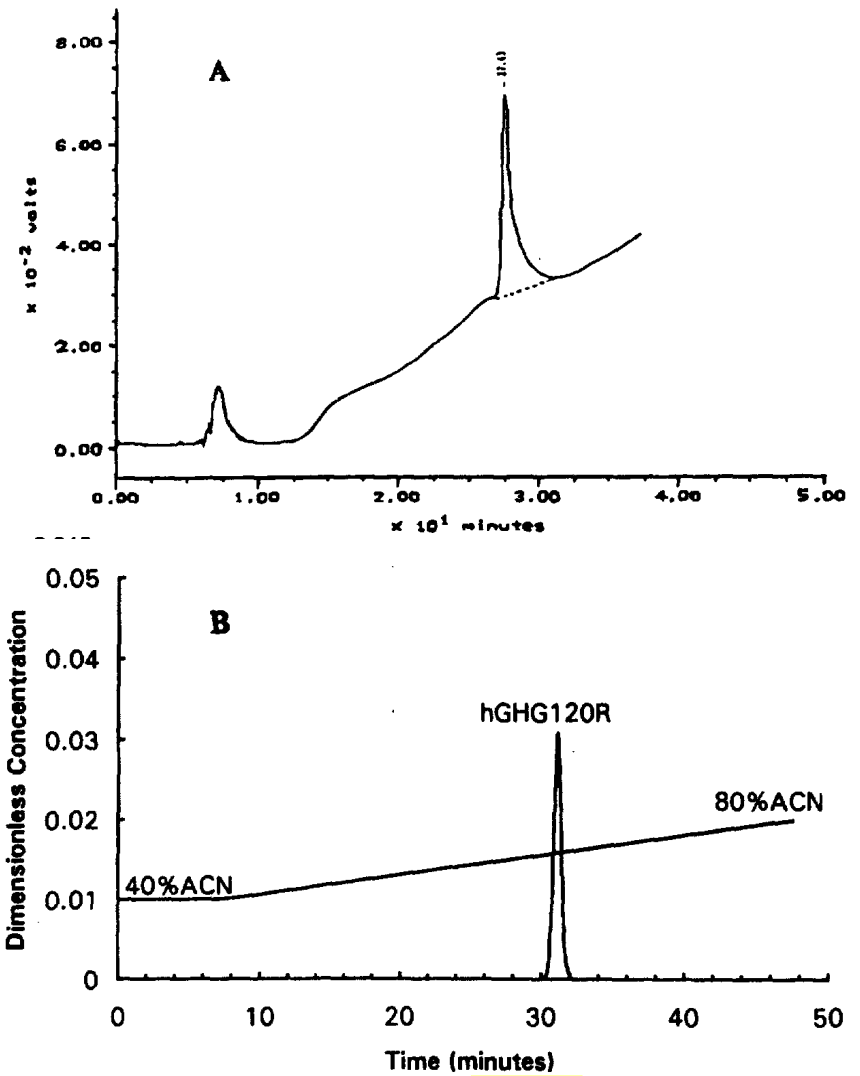

Fig. 5. Experimental and simulated chromatograms for a small hGHG120R sample on the preparative column.

several gradient runs on a preparative RP-HPLC column reasonably well. The rate model and the parameter estimation protocol presented in this work can be used for the scale-up of RP-HPLC. Gradient elution profiles can be predicted without a posteriori chromomatographic data from the preparative column. Only a small analytical column is needed to perform a few simple experiments to estimate the parameters in the eluite–modulator retention relationship and the adsorption saturation capacity. The advantages of the rate model system will be more revealing if the scale-up target is a large-scale column with significant mass transfer effects.

In practice, a scale-up project may have two options. One is buying an existing column from a vendor. Another is to custom-build a column. In the first case, computer simulations are carried out based on the specifications of the available column to predict the chromatogram for a target gradient separation. A column can then be chosen based on the simulation results. If a column has to be

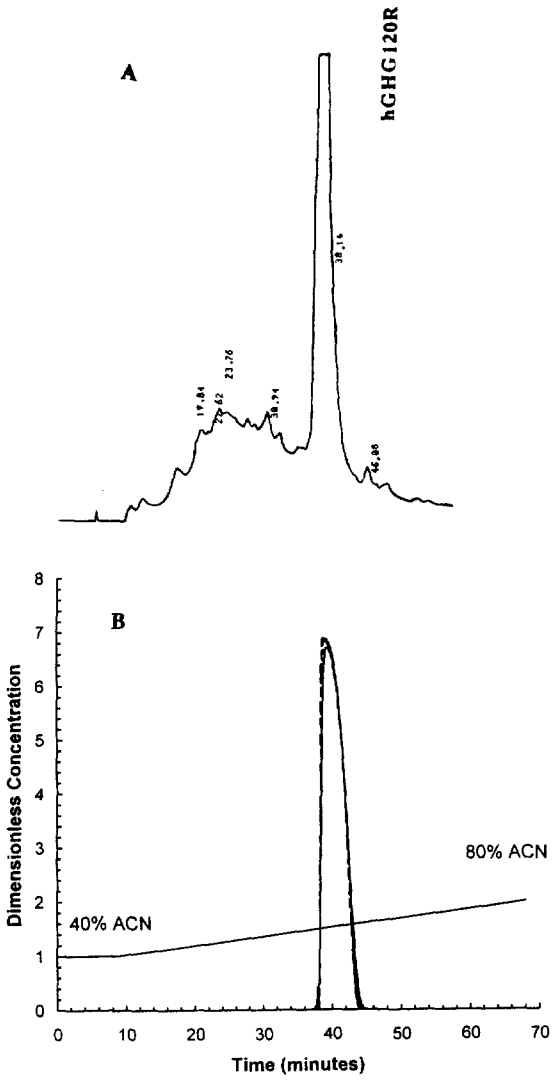

Fig. 6. Experimental and simulated chromatograms for a large hGHG120R sample on the preparative column.

custom-built, simulations can be carried out by adjusting the packing material, column size and operating parameters to predict the chromatogram for a target gradient separation. This process is repeated until computer simulation indicates that the column to be made will achieve a satisfactory performance. If a parameter is very difficult to obtain, one can fit an experimental chromatographic peak from a small column with a simulated peak to obtain the parameter.

Appendix A

7.0.1. Notation

a_i constant in Langmuir isotherm for component i, $b_i C_i^{\infty}$

b_i adsorption equilibrium constant for component i, k_{ai}/k_{di}

Bi_i Biot number of mass transfer for component i, $k_i R_p/(\epsilon_p D_{pi})$

C_{0i} concentration used for nondimensionalization, $\max\{C_{fi}(t)\}$

C_{bi} bulk-fluid phase concentration of component i

C_{fi} feed concentration profile of component i, a time-dependent variable

C_{m0} volume fraction of ACN in the mobile phase which is used to equilibrate the column

C_{pi} concentration of component i in the stagnant fluid phase inside the particle macropores

C_{pi}^{*} concentration of component i in the solid phase of the particle (based on the unit volume of the particle skeleton)

C^{∞} adsorption saturation capacity (based on the unit volume of the particle skeleton)

c_{bi} $= C_{bi}/C_{0i}$

c_{pi} $= C_{pi}/C_{0i}$

c_{pi}^{*} $= C_{pi}^{*}/C_{0i}$

c_i^{∞} $= C_i^{\infty}/C_{0i}$

D_{bi} axial or radial dispersion coefficient of component i

D_m molecular diffusivity

D_{pi} effective diffusivity of component i, porosity not included

Da_i^a Damköhler number for adsorption, $L(k_{ai}C_{0i})/v$

Da_i^d Damköhler number for desorption, Lk_{di}/v

d inner diameter of a column

k_i film mass transfer coefficient of component i

k_{ai} adsorption rate constant for component i

k_{di} desorption rate constant for component i

k_i' retention factor (capacity factor) for component i

L column length

M molecular weight of an eluite or a modulator

N number of interior collocation points

N_e number of quadratic elements

N_s number of components

Table 4
Parameters used for Fig. 6(B)[a]

Direct raw data		
V_{imp} (sample size, ml)	50	
C_{sample} (sample concentration, mol l^{-1})	8.8×10^{-6}	
ΔC_m (ACN volume fraction difference)	0.4 ($=C_{m,end}-C_{m0}=80\%-40\%$)	
t_G (gradient time, min)	60	
Q (flow rate, ml min^{-1})	2	
L (column length, cm)	25	
d_c (column diameter, cm)	1	
t_0 (solvent time, min)	2.78	See Fig. 2(A)
Gradient delay volume (ml)	174	
V_{loop} (sample loop size, ml)	2	
R_p (particle radius, cm)	2.5×10^{-4}	
τ_{tor} (tortuosity)	4	
d_p (pore diameter, Å)	300	
ϵ_b (bed voidage)	0.4	
Calculated data		
V_b ($=\pi d_c^2 L/4$, bed volume, ml)	19.63	
v (interstitial velocity, cm s^{-1})	0.106	Eq. (22)
τ_{imp} (dimensionless injection time)	6.37	Eq. (21)
ϵ_p (particle porosity)	0.45	
τ_{delay} (dimensionless delay time)	22.15	Eq. (25)
$a_1=C_{m0}-a_2(\tau_{delay}-\tau_{imp})$	−0.1333	Eq. (24)
$a_2=\Delta C_m/\Delta\tau=\Delta C_m/(t_G v/L)$	0.0262	Eq. (24)
	hGHG120R	
d_m (molecular diameter, Å)	40.35	Eq. (38)
$\lambda=d_m/d_p$	0.1345	
D_m (molecular diffusivity, $cm^2\ s^{-1}$)	9.78×10^{-7}	Eq. (39)
D_p (effect, intraparticle diffusivity, $cm^2\ s^{-1}$)	1.77×10^{-7}	Eq. (37)
k (film mass transfer coefficient, cm s^{-1})	0.0149	Eq. (42)
Pe_L (Peclet number)	25 000	Eq. (36)
$\eta=\epsilon_p D_p L/(R_p^2 v)$	299.5	
$Bi=kR_p/(\epsilon_p D_p)$, Biot number	46.8	
L/v (min)	3.927	

[a]The computer code requires the following parameters as data input: N (=2, number of components), N_e (number of finite elements, set to 22), N_c (number of interior collocation points, set to 1), τ_{imp}, ϵ_p, ϵ_b, Pe_{Li}, η_i, Bi_i, C_{0i} (set to 100% for ACN; $=C_{sample}$ for protein), C^∞, α_i, β_i, γ_i, C_{m0}, τ_{delay}, a_1 and a_2. The L/v value is needed to convert τ into real time. The values of C^∞, α_i, β_i and γ_i are listed in Table 1.

Pe_{Li} Peclet number of axial dispersion for component i, vL/D_{bi}
p empirical parameter with a value of 5/8
Q mobile phase volumetric flow rate
R radial coordinate for particle
R_p particle radius
Re Reynolds number, $(v\epsilon_b)\rho_f(2R_p)/\mu$
r $=R/R_p$
Sc Schmidt number, $\mu/(\rho_f D_m)$
Sh Sherwood number, $k(2R_p)/D_m$
t dimensional time ($t=0$ is the moment a sample enters a column)
t_0 dead volume time of unretained small molecules, such as salts and solvents
t_{adj} chromotogram recording delay time (min)
t_d dead volume time of unretained large molecules, such as blue dextrin
t_R dimensional retention time
v interstitial velocity, $4Q/(\pi d^2\epsilon_b)$
V_{loop} volume of the sample loop
$V_{s,h}$ hydrated specific volume of a protein (cm^3 per g protein)

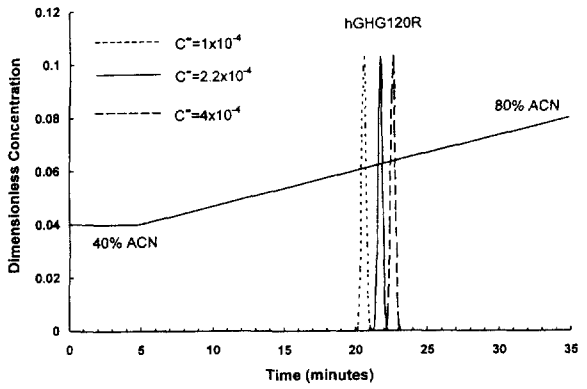

Fig. 7. Effect of the adsorption saturation capacity C^{∞}.

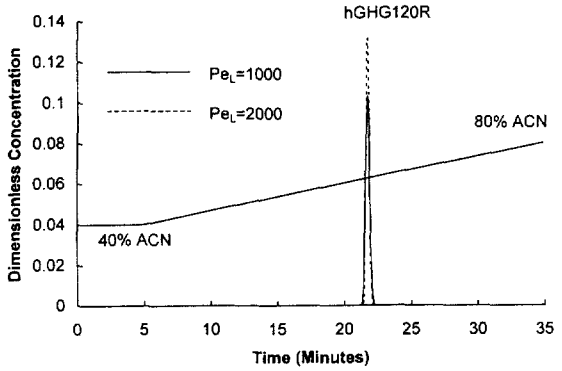

Fig. 8. Effect of the Peclet number.

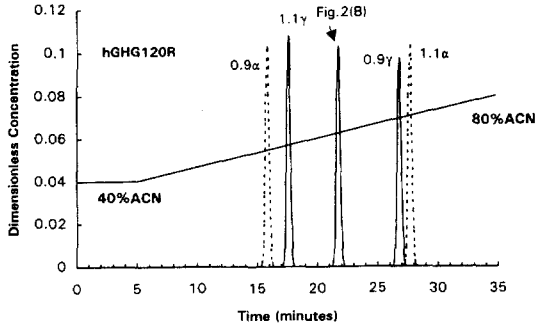

Fig. 9. Effects of 10% variations in α or γ values in the eluite–modulator relationship.

w_s column saturation capacity (mg of eluite) corresponding to a very concentrated equilibrium concentration

w_x amount of eluite (mg) in a large sample for evaluation of C^{∞}

Z axial coordinate

z dimensionless axial coordinate, Z/L

7.0.2. Greek letters

α_i, β_i, γ_i parameters for the eluite–modulator correlation

ϵ_b bed void volume fraction

ϵ_p particle porosity

η_i dimensionless constant, $\epsilon_p D_{pi} L/(R_p^2 v)$

μ mobile phase viscosity

ξ_i dimensionless constant for component i, $3Bi_i\eta_i(1-\epsilon_b)/\epsilon_b$

ρ_f mobile phase density

τ dimensionless time, vt/L

τ_{delay} dimensionless time it takes for the gradient front to reach the column inlet

τ_R dimensionless retention time

τ_{imp} dimensionless time duration for a rectangular pulse of the sample

ϕ phase ratio (staionary phase to mobile phase), $(1-\epsilon_b)(1-\epsilon_p)/[\epsilon_b+(1-\epsilon_b)\epsilon_p]$

References

[1] T. Gu, Y.-H. Truei, G.-J. Tsai, G.T. Tsao, Modeling of gradient elution in multicomponent nonlinear chromatography, Chem. Eng. Sci. 47 (1992) 253.

[2] J.E. Eble, E.L. Grob, P.E. Antle, L.R. Snyder, Simplified description of high-performance liquid chromatographic separation under overload conditions, based on the Craig distribution model, J. Chromatogr. 384 (1987) 25.

[3] S. Furusaki, E. Haruguchi, T. Nozawa, Separation of proteins by ion-exchange chromatography using gradient elution, Bioprocess Eng. 2 (1987) 49.

[4] F.D. Antia, Cs. Horvath, Gradient elution in nonlinear preparative liquid chromatography, J. Chromatogr. 484 (1989) 1.

[5] W.W. Pitts Jr.,, Gradient-elution ion exchange chromatography: a digital computer solution of the mathematical model, J. Chromatogr. Sci. 14 (1976) 396.

[6] K. Kang, B.J. McCoy, Protein separations by ion-exchange chromatography: a model for gradient elution, Biotechnol. Bioeng. 33 (1989) 786.

[7] W.R. Melander, Z.E. Rassi, Cs. Horvath, Interplay of hydrophobic and electrostatic interactions in biopolymer chromatography, J. Chromatogr. 469 (1989) 3.

[8] T. Gu, Mathematical Modeling and Scale-up of Liquid Chromatography, Springer, Berlin, 1995, pp. 96, 32–38.

[9] T. Gu, Y. Zheng, Y. Gu, R. Haldankar, N. Bhalerao, D. Ridgway, P.E. Wiehl, W.Y. Chen, J.J. Kopchick,

Purification of a pyrogen-free guman growth hormone analog hGHG120R for animal testing, Biotechnol. Bioeng. 48 (1995) 520.

[10] L.R. Snyder, J.J. Kirkland, Introduction to Modern Liquid Chromatography, Wiley, New York, 1974, p. 26.

[11] P.N. Brown, G.D. Byrne, A.C. Hindmarsh, VODE: a variable coefficient ODE solver, SIAM J. Sci. Stat. Comput. 10 (1989) 1038.

[12] K.K. Unger, Porous Silica: Its Properties and Use as Support in Column Liquid Chromatography, Elsevier, Amsterdam, 1979, p. 170.

[13] L.R. Snyder, M.A. Stadalius, Gradient elution, in: Cs. Horvath (Ed.), High-Performance Liquid Chromatography — Advances and Perspectives, vol. 4, Academic Press, New York, 1986, pp. 195–312.

[14] L.R. Snyder, G.B. Cox, P.E. Antle, Preparative separation of peptide and protein samples by high-performance liquid chromatography with gradient elution. I. The Craig model as a basis for computer simulations, J. Chromatogr. 444 (1988) 303.

[15] S.F. Chung, C.Y. Wen, Longitudinal dispersion of liquid flowing through fixed and fluidized beds, AIChE J. 14 (1968) 857.

[16] W.W. Yau, J.J. Kirkland, D.D. Bly, Modern Size Exclusion Liquid Chromatography, Wiley, New York, 1979, p. 88.

[17] C.J. Geankoplis, Transport Processes and Unit Operations, 3rd ed., Prentice Hall, Englewood Cliffs, NJ, 1993, p. 468.

[18] C.N. Satterfield, Mass Transfer in Heterogeneous Catalysis, MIT Press, Cambridge, MA, 1970.

[19] A.G. Marshall, Biophysical Chemistry: Principles, Techniques, and Applications, Wiley, New York, 1978, pp. 200–102.

[20] C.R. Cantor and P.R. Schimmel, Biophysical Chemistry, Part II: Techniques for the Study of Biological Structure and Function, W.H. Freeman, San Francisco, 1980, p. 554.

[21] A. Polson, Some aspects of diffusion in solution and a definition of a colloidal particle, J. Phys. Colloid Chem. 54 (1950) 649.

[22] D.M. Ruthven, Principles of Adsorption and Adsorption Processes, Wiley, New York, 1984, p. 214.

[23] E.J. Wilson, C.J. Geankoplis, Liquid mass transfer at very low Reynolds numbers in packed beds, Ind. Eng. Chem. Fundam. 5 (1966) 9.

[24] T. Kataoka, H. Yoshida, T. Yamada, Liquid phase mass transfer in ion exchange based on the hydraulic radius model, J. Chem. Eng. Jpn. 6 (1973) 172.

[25] Z. Li, Y. Gu, T. Gu, Mathematical modeling and scale-up of size exclusion chromatography, Biochem. Eng. J., (revised manuscript submitted for publication).